Analytical investigation of the effects of lateral connections on the accuracy of population coding

Masafumi Oizumi,[1] Keiji Miura,[2,3] and Masato Okada[1,4,*]
[1]*Department of Complexity Science and Engineering, University of Tokyo, Kashiwa-shi, Chiba, Japan*
[2]*PRESTO, Japan Science and Technology Agency, Kawaguchi-shi, Saitama, Japan*
[3]*Department of Molecular and Cellular Biology, Harvard University, Cambridge, Massachusetts 02138, USA*
[4]*Brain Science Institute, RIKEN, Wako-shi, Saitama, Japan*
(Received 31 August 2009; published 5 May 2010)

We studied how lateral connections affect the accuracy of a population code by using a model of orientation selectivity in the primary visual cortex. Investigating the effects of lateral connections on population coding is a complex problem because these connections simultaneously change the shape of tuning curves and correlations between neurons. Both of these changes caused by lateral connections have to be taken into consideration to correctly evaluate their effects. We propose a theoretical framework for analytically computing the Fisher information, which measures the accuracy of a population code, in stochastic spiking neuron models with refractory periods. Within our framework, we accurately evaluated both the changes in tuning curves and correlations caused by lateral connections and their effects on the Fisher information. We found that their effects conflicted with each other and the answer to whether or not the lateral connections increased the Fisher information strongly depended on the intrinsic properties of the model neuron. By systematically changing the coupling strengths of excitations and inhibitions, we found the parameter regions of lateral connectivities where sharpening of tuning curves through Mexican-hat connectivities led to an increase in information, which is in contrast to some previous findings.

DOI: 10.1103/PhysRevE.81.051905 PACS number(s): 87.18.Sn, 87.19.L−, 87.85.dq

I. INTRODUCTION

Information from the external and internal worlds is encoded in the noisy population activities of neurons in the brain. Understanding how this information is accurately processed is a central problem in neuroscience. The role of lateral connections for accurate information processing is of special interest. However, there is as yet no rigorous treatment of how lateral connections affect the accuracy of a population code. Because lateral connections change not only the tuning curve of each neuron but also the correlation between neuronal activities, we need to take both effects into consideration. Although the effects of changing the tuning curve and the neural correlations have been separately examined in previous studies [1–4], little light has been shed on the effect of both changes together [5,6]. In this paper, we describe a theoretical framework for evaluating the effects of lateral connections on the accuracy of a population code taking both effects into consideration. We apply the theoretical framework to a model of orientation selectivity in the primary visual cortex and discuss how lateral connections affect the accuracy of population coding.

We use the Fisher information to evaluate the accuracy of a population code [1,2,7]. The Fisher information quantifies the maximal amount of information about stimuli that can be extracted from noisy neural activities. We aim to analytically compute the Fisher information in a network model of spiking neurons by taking into consideration both changes in tuning curves and neural correlation caused by changes in lateral connections. Assuming that the fluctuations of mean firing rates obey a Gaussian distribution, we can analytically compute the Fisher information if we can compute the mean firing rates and covariance matrix of the Gaussian distribution. However, it is generally difficult to compute the correlations in a realistic spiking neuron model analytically. For this reason, the previous studies have resorted to numerical methods of computing the Fisher information [5,6].

To overcome the difficulty with computing correlations, we used the spike response model introduced by Gerstner and van Hemmen [8], where correlations can be analytically computed within the framework of mean-field theory [9,10]. The spike response model is not only analytically tractable but can also be made realistic by tuning the model parameters [8,11]. Our approach provides a powerful way of studying the effects of lateral connections on the accuracy of a population code within a realistic network model of spiking neurons.

We chose an orientation selectivity model in which short-range excitations together with longer-range inhibitions produce a Mexican-hat interaction [5,6,12,13] as a model circuit for investigating the effects of lateral connections. It has previously been reported that sharpening of tuning curves through a Mexican-hat interaction greatly reduces the accuracy of population coding in terms of the Fisher information due to the adverse effects of correlations that it induces [5,6]. However, because the authors relied on numerical methods of computing the Fisher information, their work seemed to lack an extensive search for parameters because of the substantial amount of time it takes to compute the Fisher information numerically. By systematically changing the strengths of recurrent excitations and lateral inhibitions, we found parameter regions where the sharpening of tuning curves via Mexican-hat interactions actually improved the accuracy of a population code, which is in contrast to the previous findings.

*okada@k.u-tokyo.ac.jp

II. MODEL

Let us consider a discrete time version of a spike response model with threshold noise [10,14]. The network consists of N neurons, which take two states, denoted by $S=0,1$. $S=0$ means that the neuron does not fire and $S=1$ means that the neuron fires. The states of every neuron S_i are stochastically updated in parallel. The probability that S_i takes the 0 or 1 state depends on the membrane potential, u_i

$$P[S_i(t)=1]=g[u_i(t)],$$

$$P[S_i(t)=0]=1-P[S_i(t)=1], \tag{1}$$

where g is called "the escape function" [8], which is monotonically increasing and is a differentiable function taking values between 0 and 1. The membrane potential u_i is determined by the past spike histories of N neurons,

$$u_i(t)=\sum_{\tau=1}^{\infty}\sum_{j\neq i} J_{ij}\epsilon_{ij}(\tau)S_j(t-\tau)+\eta_i(t-t_i^{(f)})+h_i+u_r, \tag{2}$$

where $\epsilon_{ij}(\tau)$ describes the time course of a postsynaptic potential evoked by the firing of presynaptic neurons and $\eta_i(\tau)$ represents the effect of refractoriness. The refractory function, η_i, only depends on the last spike of neuron i. $t_i^{(f)}$ denotes the time when the last spike of neuron i occurred. $\epsilon(\tau)$ and $\eta(\tau)$ are called the response kernels. h_i is an input potential, and u_r is the resting potential.

The advantage of the spike response model is that it is analytically tractable thanks to the linearity of the model. The correlation functions can be analytically computed in the spike response model within the framework of mean-field theory [9,10]. In addition to analytical tractability, we can make the spike response model realistic by choosing appropriate response kernels. For instance, the spike response model, according to reports, can accurately predict the timings of spikes generated with the Hodgkin-Huxley-type equation [11].

In this paper, we consider absolute refractoriness for the sake of simplicity. That is, the refractory function $\eta(\tau)$ is given by

$$\eta(\tau)=\begin{cases}-\infty & \text{for } 1\leq\tau\leq\tau_{abs}\\ 0 & \text{for } \tau>\tau_{abs},\end{cases} \tag{3}$$

where τ_{abs} is the absolute refractory period. We derive a set of closed equations for correlation functions in the spike response model with absolute refractoriness.

III. THEORY OF CORRELATIONS

A. Instantaneous firing rate

First, let us consider the noise averages of neuronal state variables denoted by $\langle S_i(t)\rangle$. We call the value, $\langle S_i(t)\rangle$, the instantaneous firing rate at time t. The noise average of some function f is defined as

$$\langle f(\mathbf{S}^t,\mathbf{S}^{t-1},\ldots,\mathbf{S}^0)\rangle \equiv \sum_{\mathbf{S}^t}\sum_{\mathbf{S}^{t-1}}\cdots\sum_{\mathbf{S}^0} f(\mathbf{S}^t,\mathbf{S}^{t-1},\ldots,\mathbf{S}^0)P(\mathbf{S}^t,\mathbf{S}^{t-1},\ldots,\mathbf{S}^0), \tag{4}$$

where $\mathbf{S}^t=\{S_1(t),S_2(t),\ldots,S_N(t)\}$ represents the spike pattern of N neurons at time t and $\Sigma_{\mathbf{S}^t}$ represents the summation over all possible configurations $\mathbf{S}^t$. $P(\mathbf{S}^t,\mathbf{S}^{t-1},\ldots,\mathbf{S}^0)$ is the probability of finding the system in a state $(\mathbf{S}^t,\mathbf{S}^{t-1},\ldots,\mathbf{S}^0)$. The joint probability $P(\mathbf{S}^t,\mathbf{S}^{t-1},\ldots,\mathbf{S}^0)$ is described by the following master equation:

$$P(\mathbf{S}^t,\mathbf{S}^{t-1},\ldots,\mathbf{S}^0) = W(\mathbf{S}^t|\mathbf{S}^{t-1},\mathbf{S}^{t-2},\ldots,\mathbf{S}^0)P(\mathbf{S}^{t-1},\mathbf{S}^{t-2},\ldots,\mathbf{S}^0), \tag{5}$$

where $W(\mathbf{S}^t|\mathbf{S}^{t-1},\mathbf{S}^{t-2},\ldots,\mathbf{S}^0)$ is called the transition probability, which is determined by the update rule [Eq. (1)],

$$W(\mathbf{S}^t|\mathbf{S}^{t-1},\mathbf{S}^{t-2},\ldots,\mathbf{S}^0)=\prod_{i=1}^{N}\frac{1+[2S_i(t)-1]\{2g[u_i(t)]-1\}}{2}. \tag{6}$$

To simplify the description, the past spike histories, $\{\mathbf{S}^{t-1},\mathbf{S}^{t-2},\ldots,\mathbf{S}^0\}$, are denoted by X^{t-1}.

By using Eq. (5), the instantaneous firing rate at time t, $\langle S_i(t)\rangle$, can be computed as

$$\langle S_i(t)\rangle=\sum_{X^{t-1}}P(X^{t-1})\sum_{\mathbf{S}^t}S_iW(\mathbf{S}^t|X^{t-1}) =\langle g[u_i(t)]\rangle, \tag{7}$$

where $\Sigma_{X^{t-1}}$ represents the summation over all possible configurations of the past spike histories X^{t-1}. Here, we denote the terms in the membrane potential u_i [Eq. (2)] which exclude the refractory term $\eta_i(t-t_i^{(f)})$ by $\hat{u}_i$, that is,

$$\hat{u}_i=\sum_{\tau=1}^{\infty}\sum_{j\neq i}J_{ij}\epsilon_{ij}(\tau)S_j(t-\tau)+h_i+u_r. \tag{8}$$

We expand $g(u_i)$ around the noise average of $\hat{u}_i$,

$$\begin{aligned}\langle S_i(t)\rangle=\langle g[\langle\hat{u}_i(t)\rangle+\eta_i(t-t_i^{(f)})]\rangle+\Big\langle g'[\langle\hat{u}_i(t)\rangle+\eta_i(t-t_i^{(f)})]\sum_{\tau=1}^{\infty}\sum_{j\neq i}^{N}J_{ij}\epsilon_{ij}(\tau)\delta S_j(t-\tau)\Big\rangle\\ +\frac{1}{2}\Big\langle g''[\langle\hat{u}_i(t)\rangle+\eta_i(t-t_i^{(f)})]\sum_{\tau=1}^{\infty}\sum_{\tau'=1}^{\infty}\sum_{j\neq i}^{N}\sum_{k\neq i}^{N}J_{ij}\epsilon_{ij}(\tau)J_{ik}\epsilon_{ik}(\tau')\delta S_j(t-\tau)\delta S_k(t-\tau')\Big\rangle+\cdots,\end{aligned} \tag{9}$$

where $\delta S_i=S_i-\langle S_i\rangle$, $g'(u)=dg(u)/du$, and $g''=d^2g(u)/du^2$. When each neuron is connected to a number of neurons of order N and connections J_{ij} are all of order $1/N$, cross correlations $\langle\delta S_i\delta S_j\rangle$ are of order $1/N$ [9]. In such a situation, the second term and the third term in Eq. (9) are of order

$1/N$. Hence, considering the limit of $N\to\infty$, one obtains to leading order,

$$\langle S_i(t)\rangle = \langle g[\langle \hat{u}_i(t)\rangle + \eta_i(t - t_i^{(f)})]\rangle. \tag{10}$$

Taking the average for the refractory function $\eta_i(t-t_i^{(f)})$, $\langle S_i(t)\rangle$ can be computed as

$$\begin{aligned}\langle S_i(t)\rangle &= \sum_{t_i'=1}^{\infty} P(t_i')g[\langle \hat{u}_i(t)\rangle + \eta_i(t_i')] \\ &= g[\langle \hat{u}_i(t)\rangle] \sum_{t_i'=\tau_{abs}+1}^{\infty} P(t_i') \\ &= g[\langle \hat{u}_i(t)\rangle]\left[1 - \sum_{t_i'=1}^{\tau_{abs}} P(t_i')\right] \\ &= g(\langle \hat{u}_i(t)\rangle)\left[1 - \sum_{t_i'=1}^{\tau_{abs}} \langle S_i(t-t_i')\rangle\right],\end{aligned} \tag{11}$$

where $t_i' = t - t_i^{(f)}$ and $P(t_i')$ is the probability that the last spike of neuron i occurred at $t-t_i'$, i.e., $P(t_i') = P[S_i(t-t_i')=1, S_i(t-t_i'+1)=0, \ldots, S_i(t-1)=0]$. Note that when $t_i' \le \tau_{abs}$, $P(t_i')$ can be simply written as $P(t_i') = P[S_i(t-t_i')=1]$ due to there being an absolute refractory period. We took advantage of this simplification in the above calculation. This property of the absolute refractory period also significantly simplifies the following correlation function calculations.

By taking the limit $t\to\infty$ in Eq. (11), the instantaneous firing rate in a stable stationary state is given by

$$\langle S_i\rangle = \frac{g(\langle \hat{u}_i\rangle)}{1 + \tau_{abs} g(\langle u_i\rangle)}. \tag{12}$$

Substituting Eq. (8) into Eq. (12), we obtain self-consistent equations of $\langle S_i\rangle$. By solving these self-consistent equations, we can compute the instantaneous firing rates at equilibrium.

B. Equal-time correlation functions

This section discusses the values of equal-time autocorrelation functions and equal-time cross-correlation functions. Autocorrelation functions are defined as

$$A_i(t, t+\tau) \equiv \langle \delta S_i(t)\, \delta S_i(t+\tau)\rangle. \tag{13}$$

We denote the autocorrelation functions at equilibrium by $A_i(\tau) \equiv \lim_{t\to\infty} A_i(t, t+\tau)$. The equilibrium value of equal-time autocorrelation functions $A_i(0)$ are simply

$$A_i(0) = \langle S_i\rangle(1 - \langle S_i\rangle). \tag{14}$$

The cross-correlation functions are defined as

$$C_{ij}(t, t+\tau) \equiv \langle \delta S_i(t)\, \delta S_j(t+\tau)\rangle, \tag{15}$$

where $i \neq j$. We denote the cross correlation functions at equilibrium by $C_{ij}(\tau) \equiv \lim_{t\to\infty} C_{ij}(t, t+\tau)$. We calculate the equilibrium value of equal-time cross correlation functions $C_{ij}(0)$ in this section. The equal-time cross correlation functions can be written as

$$\begin{aligned}C_{ij}(t,t) &= \langle S_i(t) S_j(t)\rangle - \langle S_i(t)\rangle\langle S_j(t)\rangle \\ &= \sum_{X^{t-1}} P(X^{t-1}) \sum_{\mathbf{S}^t} S_i S_j W(\mathbf{S}^t | X^{t-1}) - \langle S_i(t)\rangle\langle S_j(t)\rangle \\ &= \langle g[u_i(t)] g[u_j(t)]\rangle - \langle g(u_i)\rangle\langle g(u_j)\rangle.\end{aligned} \tag{16}$$

By expanding $g(u_i)$ around the noise average of $\hat{u}_i$ and taking the limit $t\to\infty$, we obtain the equal-time cross correlation functions $C_{ij}(t,t)$ at equilibrium (see Appendix A for details),

$$\begin{aligned}C_{ij}(0) = {} & g(\langle \hat{u}_i\rangle) g(\langle \hat{u}_j\rangle) \sum_{t_i'=1}^{\tau_{abs}} \sum_{t_j'=1}^{\tau_{abs}} C_{ij}(t_i' - t_j') + g'(\langle \hat{u}_i\rangle) g(\langle \hat{u}_j\rangle)(-1 + \tau_{abs}\langle S_i\rangle) \sum_{t_j'=1}^{\tau_{abs}} \sum_{\tau}^{\infty} \left(\sum_{k\neq i,j} J_{ik}\epsilon_{ik}(\tau) C_{kj}(\tau - t_j') + J_{ij}\epsilon_{ij}(\tau) A_j(\tau - t_j') \right) \\ & + g'(\langle \hat{u}_j\rangle) g(\langle \hat{u}_i\rangle)(-1 + \tau_{abs}\langle S_j\rangle) \sum_{t_i'=1}^{\tau_{abs}} \sum_{\tau}^{\infty} \left(\sum_{k\neq i,j} J_{jk}\epsilon_{jk}(\tau) C_{ki}(\tau - t_i') + J_{ji}\epsilon_{ji}(\tau) A_i(\tau - t_i') \right) \\ & + g'(\langle \hat{u}_i\rangle) g'(\langle \hat{u}_j\rangle)(1 - \tau_{abs}\langle S_i\rangle)(1 - \tau_{abs}\langle S_j\rangle), \\ & \left(\sum_{\tau,\tau'}^{\infty} \sum_{k\neq i} \sum_{l\neq j,k} J_{ik}\epsilon_{ik}(\tau) J_{jl}\epsilon_{jl}(\tau') C_{kl}(\tau - \tau') + \sum_{\tau,\tau'}^{\infty} \sum_{k\neq i} J_{ik}\epsilon_{ik}(\tau) J_{jk}\epsilon_{jk}(\tau') A_k(\tau - \tau') \right),\end{aligned} \tag{17}$$

where we have ignored three-point cross correlations such as $\langle \delta S_i \delta S_j \delta S_k\rangle$ and four-point cross correlations such as $\langle \delta S_i \delta S_j \delta S_k \delta S_l\rangle$ because these are of order $1/N^{3/2}$ and $1/N^2$, respectively. These equations for the equal-time cross correlations, $C_{ij}(0)$, include time-delayed cross correlations, $C_{ij}(\tau)$, and time-delayed autocorrelations, $A_i(\tau)$. Thus, to solve these equations, we need the equations for the time-delayed correlation functions, $C_{ij}(\tau)$ and $A_i(\tau)$.

C. Time-delayed correlation functions

In this section, we derive the equations for the time-delayed correlation functions, $C_{ij}(\tau)$ and $A_i(\tau)$. The time-delayed cross-correlation functions can be written as

$$C_{ij}(t,t+\tau) = \langle S_i(t)S_j(t+\tau)\rangle - \langle S_i(t)\rangle\langle S_j(t+\tau)\rangle$$

$$= \sum_{X^{t+\tau-1}} P(X^{t+\tau-1})S_i(t)\sum_{\mathbf{S}^{t+\tau}} S_j(t+\tau)W(\mathbf{S}^{t+\tau}|X^{t+\tau-1}) - \langle S_i(t)\rangle\langle S_j(t+\tau)\rangle$$

$$= \langle S_i(t)g[u_j(t+\tau)]\rangle - \langle g[u_i(t)]\rangle\langle g[u_j(t+\tau)]\rangle \quad (18)$$

$$= \langle \delta S_i(t)g[u_j(t+\tau)]\rangle. \quad (19)$$

By expanding $g(u_i)$ around the noise average of $\hat{u}_i$ and taking the limit $t\to\infty$, the time-delayed cross correlations at equilibrium can be written as

$$C_{ij}(\tau) = -g(\langle\hat{u}_j\rangle)\sum_{t_j'=1}^{\tau_{abs}} C_{ij}(\tau-t_j') + (1-\tau_{abs}\langle S_j\rangle)g'(\langle\hat{u}_j\rangle) \times\sum_{\tau'}^{\infty}\left(\sum_{k\neq j,i} J_{jk}\epsilon_{jk}(\tau')C_{ik}(\tau-\tau') + J_{ji}A_i(\tau-\tau')\right). \quad (20)$$

If we set $j=i$ in Eq. (20), we obtain the equations for time-delayed autocorrelations at equilibrium,

$$A_i(\tau) = -g(\langle\hat{u}_i\rangle)\sum_{t_j'=1}^{\tau_{abs}} A_i(\tau-t_j'), \quad (21)$$

where we have ignored the terms which are of order $1/N$ because $A_i(\tau)$ is of order 1. Solving Eqs. (17), (20), and (21), we eventually obtain the equilibrium value for equal-time cross correlations $C_{ij}(0)$, time-delayed cross correlations $C_{ij}(\tau)$, and time-delayed autocorrelations $A_i(\tau)$.

D. Correlations of mean firing rate

We calculated the correlations of spikes, $\langle\delta S_i\delta S_j\rangle$, in the previous sections. In this section, we compute the correlations of mean firing rates within a time window T, $Q_{ij}=\langle\delta r_i\delta r_j\rangle$, where $\delta r_i\equiv r_i-\langle r_i\rangle$, because we need these to compute the Fisher information, as will be explained in the next section. The mean firing rate, r_i, within T is defined as

$$r_i = \frac{1}{T}\sum_{\tau=1}^{T} S_i(\tau). \quad (22)$$

The correlations for the mean firing rates can be calculated as [15]

$$Q_{ij} = \langle\delta r_i\delta r_j\rangle = \langle(r_i-f_i)(r_j-f_j)\rangle = \left\langle\left(\frac{1}{T}\sum_{\tau=1}^{T} S_i(\tau)-f_i\right)\left(\frac{1}{T}\sum_{\tau'=1}^{T} S_i(\tau')-f_j\right)\right\rangle$$

$$= \frac{1}{T^2}\sum_{\tau=1}^{T}\sum_{\tau'=1}^{T}\langle S_i(\tau)S_j(\tau')\rangle - f_if_j$$

$$= \frac{1}{T^2}\sum_{\tau=1}^{T}\sum_{\tau'=1}^{T}[\langle\delta S_i(\tau)\delta S_j(\tau')\rangle + \langle S_i(\tau)\rangle\langle S_j(\tau')\rangle] - f_if_j$$

$$= \frac{1}{T^2}\sum_{\tau=1}^{T}\sum_{\tau'=1}^{T} C_{ij}(\tau'-\tau). \quad (23)$$

where $f_i=\langle r_i\rangle$. Thus, using spike correlations $C_{ij}(\tau)$, the mean firing rate correlations, Q_{ij}, can be computed through Eq. (23). Figure 8 illustrates a numerical verification of the analytical computations. The mean firing rates and correlation functions computed from the theory match to those obtained by simulating a network of spike response models.

IV. FISHER INFORMATION

Let us consider the problem of how accurately the stimulus θ, which is a single variable, can be estimated from the mean firing rates of a neuronal population $\mathbf{r}=\{r_1,r_2,\ldots,r_N\}$. Through the Cramér-Rao bound, the average squared decoding error for an unbiased estimate of a stimulus, $\hat{\theta}$, is greater than or equal to $1/I(\theta)$,

$$\langle(\theta-\hat{\theta})^2\rangle \geq \frac{1}{I(\theta)}, \quad (24)$$

where $I(\theta)$ is the Fisher information. The Fisher information is given by

$$I(\theta) = \int d\mathbf{r}P[\mathbf{r}|\theta]\left(-\frac{\partial^2 \ln P[\mathbf{r}|\theta]}{\partial\theta^2}\right), \quad (25)$$

where $P[\mathbf{r}|\theta]$ is the conditional probability distribution, which is the probability that a neural response, $\mathbf{r}$, will be evoked by the presentation of a stimulus θ. We assume that $P[\mathbf{r}|\theta]$ can be sufficiently approximated with a multivariate Gaussian probability distribution with a covariance matrix, $\mathbf{Q}(\theta)$,

$$P[\mathbf{r}|\theta] = \frac{1}{\sqrt{(2\pi)^N\det\mathbf{Q}(\theta)}} \times\exp\left\{-\frac{1}{2}[\mathbf{r}-\mathbf{f}(\theta)]^T\mathbf{Q}^{-1}(\theta)[\mathbf{r}-\mathbf{f}(\theta)]\right\}, \quad (26)$$

where $\mathbf{f}$ is the mean value of $\mathbf{r}$. Note that the (i,j)th element of covariance matrix Q_{ij} represents the mean firing rate correlation $\langle\delta r_i\delta r_j\rangle$. Under this assumption, the Fisher information can be written as [16]

$$I(\theta) = I_{\text{mean}}(\theta) + I_{\text{cov}}(\theta), \quad (27)$$

$$I_{\text{mean}}(\theta) = \mathbf{f}'(\theta)^T\mathbf{Q}^{-1}(\theta)\mathbf{f}'(\theta), \quad (28)$$

$$I_{\text{cov}}(\theta) = \text{Tr}[\mathbf{Q}'(\theta)\mathbf{Q}^{-1}(\theta)\mathbf{Q}'(\theta)\mathbf{Q}^{-1}(\theta)]/2, \quad (29)$$

where Tr stands for the trace operation, $f'(\theta)=df(\theta)/d\theta$, and $\mathbf{Q}'(\theta)=d\mathbf{Q}'(\theta)/d\theta$. Because the mean firing rate correla-

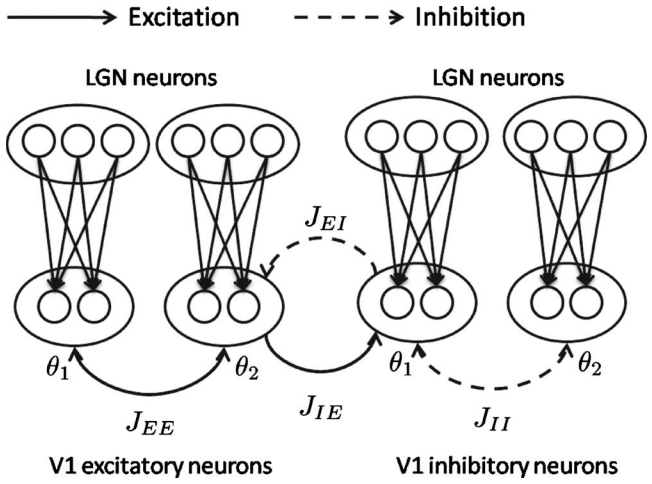

FIG. 1. Network model of orientation selectivity in primary visual cortex.

tions, Q_{ij}, can be analytically calculated in the spike response model [Eq. (23)], the Fisher information can also be analytically calculated from Eq. (27).

V. NETWORK MODEL OF ORIENTATION SELECTIVITY IN PRIMARY VISUAL CORTEX

Let us consider a network consisting of $N_E=2000$ V1 excitatory neurons, $N_I=2000$ V1 inhibitory neurons, and $N_L=4000$ LGN excitatory neurons as a model of orientation selectivity. The number of neurons was set so that the mean-field approximation is valid. If the number of neurons is enough large to satisfy the mean-field approximation, the number does not qualitatively affect the results. The diagram for this network is shown in Fig. 1. Both excitatory neurons and inhibitory neurons in V1 are selective to the orientation of bar stimuli in their common receptive field.

We assume that LGN neurons are also orientation selective and that they project to V1 neurons with the same orientation preference although LGN neurons are usually considered to be not orientation selective. It is usually assumed that the receptive fields of LGN neurons are similar to those of retinal ganglion cells, i.e., they are circular. For instance, it is assumed that there are two kinds of LGN neurons, i.e., ON center-surround cells and OFF center-surround cells. In the Hubel-Wiesel model of orientation selectivity [17], the receptive field structure of V1 neurons is established by summing the input from appropriately selected LGN neurons. With this process, the sum of LGN inputs becomes orientation selective. In the present paper, we ignored this process of generating orientation selectivity of V1 neurons because of the computational cost of analytically computing correlations. We simply emulated the sum of LGN inputs by considering the upstream neurons, which are already orientation selective. We call these upstream neurons "LGN neurons" for convenience sake.

The reason we considered the upstream neurons ("LGN neurons") is that the input to V1 neurons has to be noisy. If the input to V1 neurons is noisy, the amount of information in the V1 layer never exceeds that in the LGN layer because of the data processing inequality of information theory [18]. In contrast, if the input to V1 neurons is noiseless, the amount of information in the V1 layer is not bounded from above. This is an unrealistic situation. In the present paper, we simply emulated noisy orientation selective inputs to V1 neurons and did not take into consideration the property of the receptive fields of real LGN neurons.

Excitatory neurons are divided into $K_E=20$ subpopulations and inhibitory neurons are divided into $K_I=20$ subpopulations. The choice of the number of subpopulations does not qualitatively affect the results. All neurons in each population have the same orientation preference. The number of excitatory neurons in each population is $G_E=100$, and the number of inhibitory neurons in each population is $G_I=100$. The preferred orientations for excitatory neurons in the kth population are denoted by θ_{Ek}, and those for inhibitory neurons are denoted by θ_{Ik}. We assume that the preferred orientations are evenly distributed from $-\pi/2$ to $\pi/2$, i.e., $\theta_{Ek}=-\pi/2+k\pi/K_E$ and $\theta_{Ik}=-\pi/2+k\pi/K_I$. Neurons in V1 are connected in an all-to-all manner. The strength of connections J_{kl} between a neuron in the kth population and a neuron in the lth population is a Gaussian function of the difference in their preferred orientations. The width of this Gaussian is $\sigma_E=\pi/10$ for excitatory projections and $\sigma_I=\pi/3$ for inhibitory projections. All types of connections we consider in the V1 network are given by

$$J_{kl}=J_{EE}/N_E \exp[-\mathrm{dif}(\theta_{Ek},\theta_{El})^2/\sigma_E^2] \quad (E\to E), \tag{30}$$

$$J_{kl}=-J_{EI}/N_I \exp[-\mathrm{dif}(\theta_{Ek},\theta_{Il})^2/\sigma_I^2] \quad (I\to E), \tag{31}$$

$$J_{kl}=J_{IE}/N_E \exp[-\mathrm{dif}(\theta_{Ik},\theta_{El})^2/\sigma_E^2] \quad (E\to I), \tag{32}$$

$$J_{kl}=-J_{II}/N_I \exp[-\mathrm{dif}(\theta_{Ik},\theta_{Il})^2/\sigma_I^2] \quad (I\to I), \tag{33}$$

where $\mathrm{dif}(\theta_i,\theta_j)$ means that if $|\theta_i-\theta_j|<\pi/2$, $\mathrm{dif}(\theta_i,\theta_j)=|\theta_i-\theta_j|$ and if $|\theta_i-\theta_j|>\pi/2$, $\mathrm{dif}(\theta_i,\theta_j)=\pi-|\theta_i-\theta_j|$. J_{EE} is a parameter of the overall strength of the excitatory projections from excitatory neurons to excitatory neurons, and J_{EI}, J_{IE}, and J_{II} are parameters similar to J_{EE}. We do not consider feedback connections from V1 to LGN neurons.

LGN excitatory neurons are divided into K_L subpopulations. The number of LGN neurons in each population is $G_L=100$. The total number of LGN neurons is $N_L=G_LK_L$. Each population of LGN neurons projects to one corresponding population of V1 excitatory neurons or V1 inhibitory neurons with the same orientation preference (Fig. 1). Thus, the number of subpopulations K_L is equal to the sum of subpopulations in V1 neurons, which is K_E+K_I. The connections between LGN neurons in one population and V1 neurons in the corresponding population are all-to-all connections. The strengths of connections from LGN neurons to V1 excitatory neurons and inhibitory neurons are constant and correspond to J_{EL}/G_L and J_{IL}/G_L. The population of LGN neurons that projects to the kth population of excitatory neurons is indexed by Ek and the population of LGN neurons that projects to the kth population of inhibitory neurons is indexed by Ik. When the orientation of stimuli is ϕ, the input

potential of LGN neurons in the Ekth population, which project to excitatory neurons in the kth population, is given by

$$h(\phi)_{Ek} = h_0 \exp(a\{\cos[2(\theta_{Ek} - \phi)] - 1\}), \quad (34)$$

where h_0 is the strength of the input potential and a controls the width of the input orientation tuning curve.

Similarly, the input potential of LGN neurons in the Ikth population is given by

$$h(\phi)_{Ik} = h_0 \exp(a\{\cos[2(\theta_{Ik} - \phi)] - 1\}). \quad (35)$$

Note that V1 neurons receive noisy inputs from LGN neurons because LGN neurons stochastically fire according to the input potential, $h(\phi)_{Ek}$ or $h(\phi)_{Ik}$.

VI. EFFECTS OF LATERAL CONNECTIONS ON THE AMOUNT OF INFORMATION

We shall investigate how lateral connections affect the amount of information contained in the population activity of V1 excitatory neurons. We will not discuss the information contained in the activity of inhibitory neurons because they do not project out of V1. The network model of orientation selectivity was described in the previous section. Each neuron in the network is modeled as the discrete spike response model (see Sec. II). The response kernels of the discrete spike response model are given by $\epsilon_{ij}(\tau)=[1-\exp(-1/\tau_s)]\exp(-\tau/\tau_s)$, where $\tau_s=2$. The absolute refractory period of the refractory function, $\eta(\tau)$, which is defined by Eq. (3), is $\tau_{abs}=2$. The orientation of the stimulus is $\phi=0$. The time window, T, over which mean firing rates are computed is set to be sufficiently large, i.e., $T=1000$, to ensure that the mean firing rates obey Gaussian statistics. We verified the analytical computation of the Fisher information under the Gaussian assumption by empirically estimating the Fisher information from data sampled from the network model (see Appendix B for details). The above parameters above are fixed in all calculations discussed in this paper.

Here, to visualize the $\mathbf{Q}$ of V1 excitatory neurons, let us introduce a $K_E \times K_E$ matrix, $\mathbf{Q}_E$, where K_E is the number of subpopulations in V1 excitatory neurons. Because the correlations between two neurons are only determined by the difference in their preferred orientations, the correlations between a neuron in the kth population of excitatory neurons and a neuron in the lth population of excitatory neurons are the same. Thus, the matrix, $\mathbf{Q}$, can be written as a $K_E \times K_E$ block matrix. $\mathbf{Q}_E$ is this reduced matrix of $\mathbf{Q}$. The elements of $\mathbf{Q}_E$, $Q_{E,kl}$ stand for the mean firing rate correlations between a neuron in the kth population of excitatory neurons and a neuron in the lth population of excitatory neurons;

$$Q_{E,kl} = Q_{ij}, \quad (\forall\ i \text{ in the } k\text{th population and } \forall\ j \text{ in the } l\text{th population}). \quad (36)$$

Note that $\mathbf{Q}_E$ does not contain diagonal elements of $\mathbf{Q}$. We also introduce a similar $K_E \times K_E$ matrix $\mathbf{Q}_E^{-1}$, which consists of off-diagonal elements of $\mathbf{Q}^{-1}$ of V1 excitatory neurons,

$$(Q_E^{-1})_{kl} = (Q^{-1})_{ij}, \quad (\forall\ i \text{ in the } k\text{th population and } \forall\ j \text{ in the } l\text{th population}). \quad (37)$$

We will present $\mathbf{Q}_E$ and $\mathbf{Q}_E^{-1}$ as figures instead of matrices, $\mathbf{Q}$ and $\mathbf{Q}^{-1}$.

We consider two kinds of escape function, $g(u)$ in Eq. (1), which determine the firing probability. The first is a sigmoid function, $g(u)=[1+\tanh(\alpha u)]/2$. The second is a threshold-linear function, i.e., $g(u)=0$ for $u<0$, $g(u)=\beta u$ for $u\geq 0$, and $g(u)=1$ for $u\geq 1/\beta$. As explained below, how lateral connections affect the accuracy of a population code differs between these escape functions.

A. Case of sigmoid function

First, let us consider the case of the sigmoid function, $g(u)=[1+\tanh(\alpha u)]/2$. The parameters are as follows. α in the sigmoid function is $\alpha=2$. The resting potential is $u_r=-1.2$ in Eq. (2). In Eqs. (34) and (35), a, which determines the width of the tuning curve in LGN neurons, is $a=0.4$, and the strength of the input potential is $h_0=1.5$. The Fisher information in the LGN layer was 1.24×10^6. Since we did not change the tuning curve for the LGN neurons, the Fisher information in the LGN layer was fixed. Note that the Fisher information in the V1 layer never exceeds that in the LGN layer because of the data processing inequality of information theory [18]. The strength of the excitatory connections to inhibitory neurons is $J_{IE}=20$, and the strength of the recurrent inhibitions is $J_{II}=5$. The strength of connections from LGN neurons to V1 excitatory neurons is $J_{EL}=1.0$, and the strength of connections from LGN neurons to V1 inhibitory neurons is $J_{IL}=1.0$. J_{IE}, J_{II}, J_{EL}, and J_{IL} are fixed in the following calculations. We changed the strength of the recurrent excitations, J_{EE}, and the strength of the lateral inhibitions, J_{EI}, and we investigated what effects these had on the accuracy of a population code.

We shall separately study what effects recurrent excitations and lateral inhibitions had on the Fisher information to clarify their respective effects. First, let us consider what effects the recurrent excitations had on the Fisher information. As mentioned in Sec. IV, the Fisher information can be analytically computed by using Eq. (27). Figure 2(a) shows the Fisher information when the strength of the recurrent excitations, J_{EE}, varies. We can see that the Fisher information increases as J_{EE} increases. To understand why the recurrent excitations increase the Fisher information, let us focus on the first term of the Fisher information, $I_{\mathrm{mean}}=\mathbf{f}'(\theta)^T\mathbf{Q}^{-1}(\theta)\mathbf{f}'(\theta)$, because I_{mean} is dominant in our model [see Figs. 2(a), 3(a), 5(a), and 6(a)]. I_{mean} depends on the derivatives of mean firing rates $\mathbf{f}'$ and the inverse of the covariance matrix $\mathbf{Q}^{-1}$. Because recurrent excitations change both $\mathbf{f}'$ and $\mathbf{Q}^{-1}$, we have to take both changes into consideration.

Now we shall consider how $\mathbf{Q}^{-1}$ affects the Fisher information. Figures 2(d) and 2(e) show the off-diagonal elements of the covariance matrix, $\mathbf{Q}$, and those of the inverse of the covariance matrix, $\mathbf{Q}^{-1}$, when recurrent excitations are present. When locally positive correlations are induced by recurrent excitations [Fig. 2(d)], the off-diagonal elements of

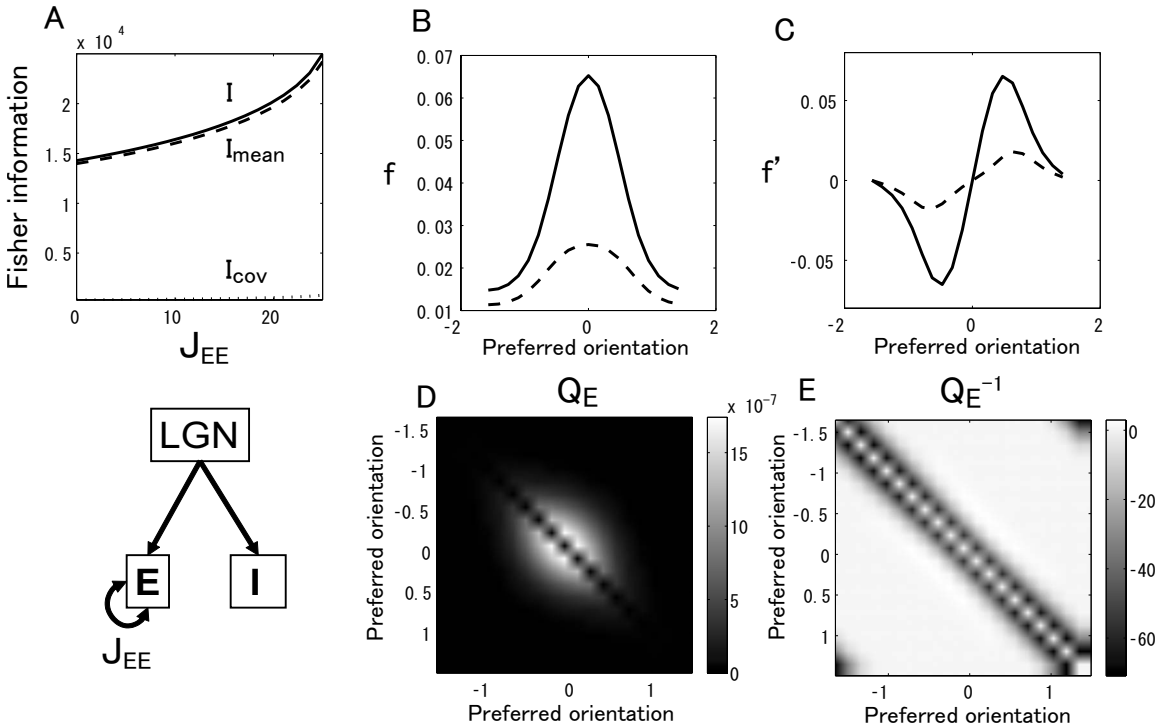

FIG. 2. (a) Effects of recurrent excitations on Fisher information when the escape function is a sigmoid function. J_{EI} is set to 0. Solid line: Fisher information I, dashed line: I_{mean}, and dotted line: I_{cov}. [(b) and (c)] Mean firing rates, (b) $\mathbf{f}$, and derivatives of mean firing rates, (c) $\mathbf{f}'$, of V1 excitatory neurons. Solid lines plot $\mathbf{f}$ and $\mathbf{f}'$ when J_{EE}=25.0. Dashed lines plot $\mathbf{f}$ and $\mathbf{f}'$ when there is no recurrent excitation, i.e., J_{EE}=0. [(d) and (e)] Grayscale plots of covariance matrix, (d) $\mathbf{Q}_E$, and inverse of covariance matrix, (e)$\mathbf{Q}_E^{-1}$, of V1 excitatory neurons when J_{EE}=25.0. Note that scales of gray color maps are different in panels (d) and (e). Diagonal elements were set to 0 to enable visualization.

$\mathbf{Q}^{-1}$ near the diagonal elements are negative [Fig. 2(e)]. We can see from I_{mean} in Eq. (28) that these locally negative off-diagonal elements decrease the Fisher information if the tuning curves, $\mathbf{f}$, are fixed. A previous paper [3] has shown that locally positive correlations decrease the Fisher information. Thus, if we only take into account the effects of recurrent excitations on correlation structures, recurrent excitations decrease the Fisher information.

Second, let us consider what effects a change in the tuning curves has on the Fisher information. Figure 2(c) shows the change in $\mathbf{f}'$ caused by recurrent excitations. We can see that recurrent excitations increase the overall amplitude of $\mathbf{f}'$. Thus, we can understand from I_{mean} that the changes in the tuning curves caused by recurrent excitations increase the Fisher information when correlations are fixed. As a result, the effects of the derivatives of the tuning curves, $\mathbf{f}'$, on the Fisher information are opposite to the effects of the correlations. Whether the Fisher information increases or not as a combinational effect is determined by which effects are stronger. In this case, the beneficial effects of the derivatives of the tuning curves on the Fisher information overcome the adverse effects of correlations and result in increased Fisher information.

Next, let us consider what effects lateral inhibitions have on the Fisher information. Figure 3(a) shows the Fisher information when the strength of the lateral inhibitions, J_{EI}, varies. In contrast to the case of recurrent excitations, the lateral inhibitions decrease the Fisher information. Let us consider why the Fisher information is decreased by the lateral inhibitions from the viewpoint of I_{mean}. Figures 3(d) and 3(e) show the off-diagonal elements of $\mathbf{Q}$ and those of $\mathbf{Q}^{-1}$ when lateral inhibitions are present. When locally negative correlations are induced by lateral inhibitions [Fig. 3(d)], the off-diagonal elements of $\mathbf{Q}^{-1}$ near the diagonal elements are positive [Fig. 3(e)]. These locally positive off-diagonal elements increase the Fisher information when the tuning curves are fixed [3]. Figure 3(c) shows the changes in the tuning curves caused by lateral inhibitions. We can see that the overall amplitude of $\mathbf{f}'$ is decreased by lateral inhibitions. Thus, the change in $\mathbf{f}'$ caused by lateral inhibitions decreases the Fisher information. Similar to the case of recurrent excitations, the change in the derivatives of the tuning curves and correlations have conflicting effects on the Fisher information. In this case, the effect of the changes in $\mathbf{f}'$ is more prominent and lead to a decrease in the Fisher information.

Finally, we investigated how excitations and inhibitions affect the accuracy of a population code as a combinational effect. Figure 4(a) shows how much the Fisher information increases or decreases compared with the Fisher information obtained in the network without lateral connections when the strength of the recurrent excitations, J_{EE}, and the strength of the lateral inhibitions, J_{EI}, vary. In the explored parameter regions in Fig. 4, the so-called marginal phase [12,19], where pure recurrent interactions can sustain localized activity with a tuning width invariant to the stimulus contrast, was not included. From Fig. 4(a), we can see that the Fisher information increases as J_{EE} increases and the Fisher information decreases as J_{EI} increases. Figure 4(b) shows how much the

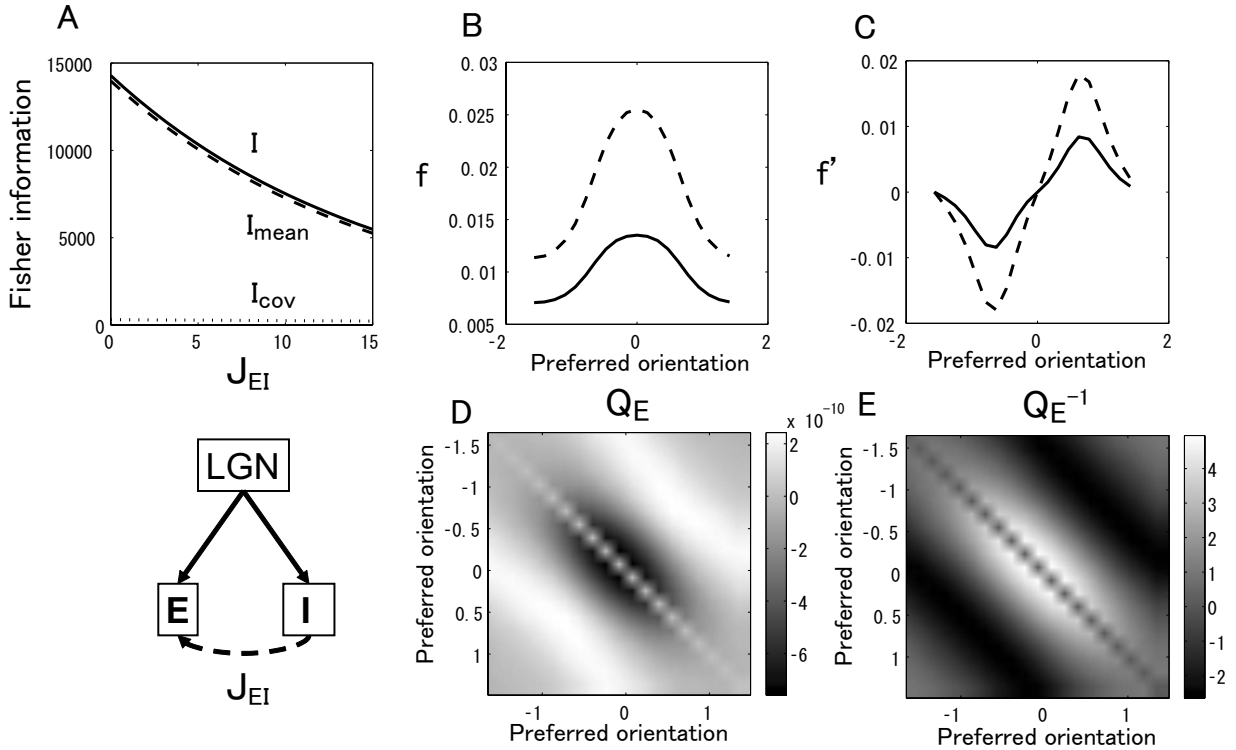

FIG. 3. (a) Effects of lateral inhibitions on Fisher information when the escape function is a sigmoid function. J_{EE} is set to 0. Solid line: Fisher information I, dashed line: I_{mean}, and dotted line: I_{cov}. [(b) and (c)] Mean firing rates, (b) $\mathbf{f}$, and derivatives of mean firing rates, (c) $\mathbf{f}'$, of V1 excitatory neurons. Solid lines plot $\mathbf{f}$ and $\mathbf{f}'$ when connection parameters are J_{EI}=15.0. Dashed lines plot $\mathbf{f}$ and $\mathbf{f}'$ when there is no lateral inhibition, i.e., J_{EI}=0. [(d) and (e)] Grayscale plots of covariance matrix, (d) $\mathbf{Q}_E$, and inverse of covariance matrix, (e) $\mathbf{Q}_E^{-1}$, of V1 excitatory neurons when J_{EI}=15.0. Diagonal elements are set to 0 to enable visualization. Note that scales of gray color maps are different in panels (d) and (e).

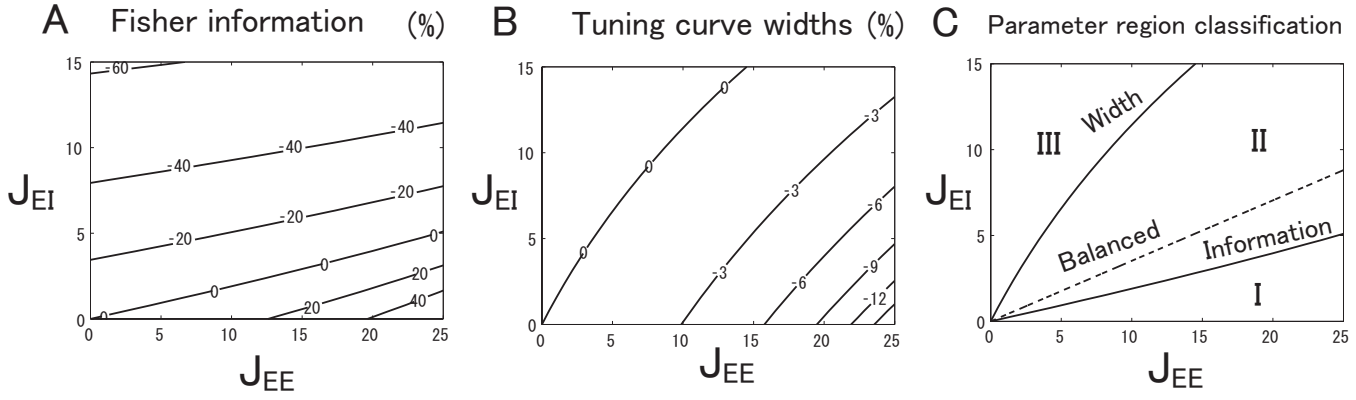

FIG. 4. Sigmoid escape function case. (a) Contour plots of Fisher information when strengths of recurrent connections and lateral inhibitions, J_{EE} and J_{EI}, varied. Values on contour lines indicate percent increase or decrease in information compared with that obtained for network without lateral connections (J_{EE}=J_{EI}=0). (b) Contour plots of tuning curve widths when strengths of recurrent connections and lateral inhibitions, J_{EE} and J_{EI}, varied. Values on contour lines indicate percent increase or decrease in width compared with that obtained for network without lateral connections (J_{EE}=J_{EI}=0). Fitting of tuning curves with a Gaussian function, $f=f_0\exp(\theta^2/\sigma^2)+C$, gave σ as width of tuning curves. (c) Classification of parameter regions based on Fisher information and tuning curve widths. Two solid lines are contour line of Fisher information (panel A) when there was no increase or decrease when strengths of recurrent connections and lateral inhibitions varied and of tuning curve widths (panel B) when there was no increase or decrease. In region I, Fisher information increases and the tuning curves get sharper. In region II, the Fisher information decreases and tuning curves get sharper. In region III, Fisher information decreases and tuning curves get broader. Dashed line indicates point at which peak firing rate of tuning curves does not change, i.e., point at which excitation and inhibition are balanced. Within parameter regions below dashed line, excitation is dominant. Within parameter regions above dashed line, inhibition is dominant.

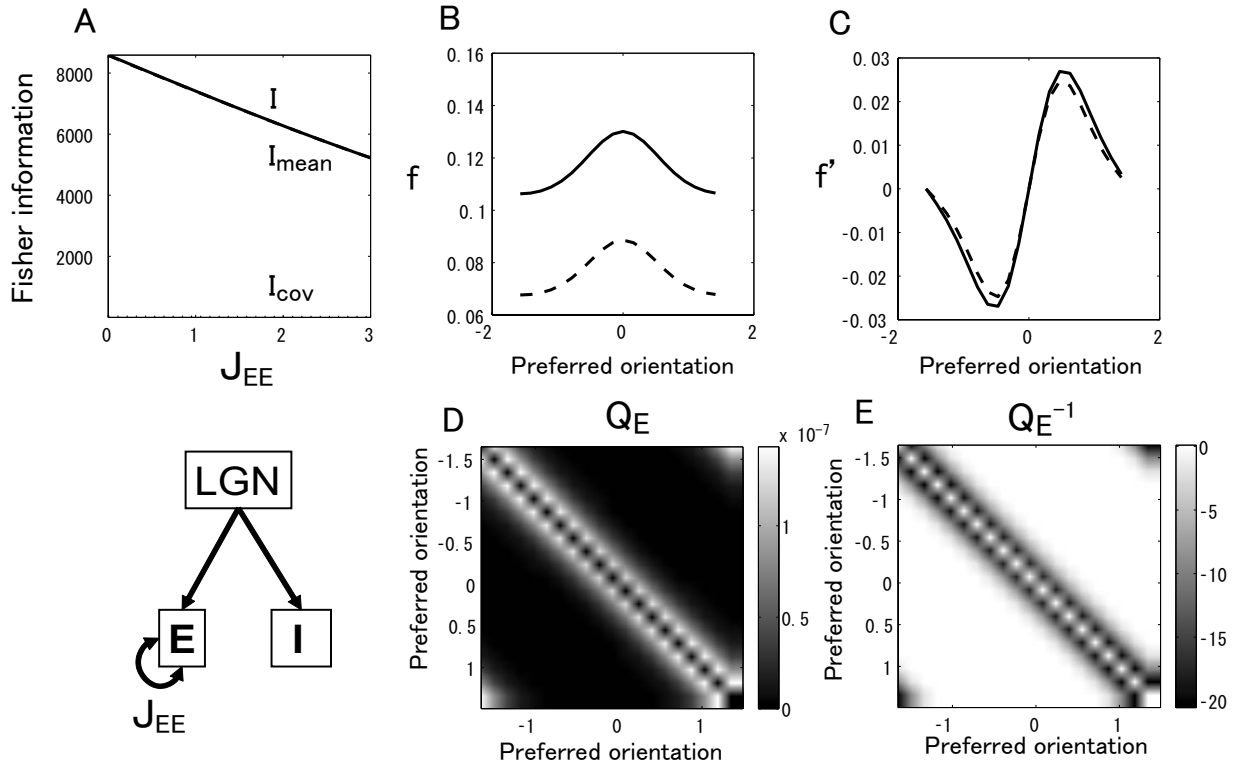

FIG. 5. (a) Effects of recurrent excitations on Fisher information when the escape function is a threshold-linear function. J_{EI} is set to 0. Solid line: Fisher information I, dashed line: I_{mean}, and dotted line: I_{cov}. [(b) and (c)] Mean firing rates, (a) $\mathbf{f}$, and derivatives of mean firing rates, (b) $\mathbf{f}'$, of V1 excitatory neurons. Solid lines plot $\mathbf{f}$ and $\mathbf{f}'$ when $J_{EE}=3.0$. Dashed lines plot $\mathbf{f}$ and $\mathbf{f}'$ when there is no recurrent excitation, $J_{EE}=0$. [(d) and (e)] Grayscale plots of covariance matrix, (d) $\mathbf{Q}_E$, and inverse of covariance matrix, (e) $\mathbf{Q}_E^{-1}$, of V1 excitatory neurons when $J_{EE}=3.0$. Diagonal elements were set to 0 to enable visualization. Note that scales of gray color maps are different in panels (d) and (e).

width of the tuning curves of V1 excitatory neurons is sharpened or broadened by lateral connections. As shown in Fig. 4(b), the recurrent excitations sharpen the tuning curves and the lateral inhibitions broaden the tuning curves. However, in most parameter regions, the tuning curves are sharpened. Several previous studies found that sharpening of tuning curves through Mexican-hat type lateral connections leads to a severe loss in information due to the adverse effects of correlations induced by lateral connections [5,6]. In contrast, Fig. 4(c) shows that there is a parameter region where the Fisher information increases when sharpening occurs (region I). In this region, excitation is stronger than inhibition (see discussion). In another parameter region (region II), the Fisher information decreases when the tuning curves are sharpened, as was shown in previous studies [5,6]. Parameter regions where excitatory input and inhibitory input are balanced [20,21] are included in region II. Whether or not the Fisher information increases is not determined by the width of the tuning curves but by the complex interplay between the derivatives of the tuning curves, $\mathbf{f}'$, and the correlations, $\mathbf{Q}$.

B. Case of threshold-linear function

Next, let us consider the case of a threshold-linear function, i.e., $g(u)=0$ for $u<0$, $g(u)=\beta u$ for $u\geq 0$, and $g(u)=1$ for $u\geq 1/\beta$. The parameters are as follows. β in the linear function is $\beta=1$. The resting potential is $u_r=0.05$. In Eqs. (34) and (35), a, which determines the width of the tuning curve in LGN neurons, is $a=1$, and the strength of the input potential is $h_0=0.1$. The Fisher information in the LGN layer was 6.82×10^4. The strength of the excitatory connections to inhibitory neurons is $J_{IE}=10$, and the strength of the recurrent inhibitions is $J_{II}=1$. The strength of connections from LGN neurons to V1 excitatory neurons is $J_{EL}=0.5$, and the strength of connections from LGN neurons to V1 inhibitory neurons is $J_{IL}=0.5$. J_{IE}, J_{II}, J_{EL}, and J_{IL} are fixed in the following calculations. We changed the strength of the recurrent excitations, J_{EE}, and the strength of the lateral inhibitions, J_{EI}, and investigated their effects on the accuracy of population codes.

As in the case of the sigmoid function, we first separately investigate what effects recurrent excitations and lateral inhibitions had on the Fisher information. Figure 5(a) shows the Fisher information when the strength of the recurrent excitations, J_{EE}, varies. In contrast to the case of the sigmoid function, the recurrent excitations decrease the Fisher information. If we compare Figs. 5(b)–5(e) with Figs. 2(b)–2(e), we can see that the changes in $\mathbf{f}'$ and correlation structures induced by recurrent excitations are basically the same as for the sigmoid function. Thus, for the same reason as in the sigmoid function case, the change in $\mathbf{f}'$ increases the Fisher information and the correlations decrease the Fisher information. However, for the threshold-linear function, the adverse

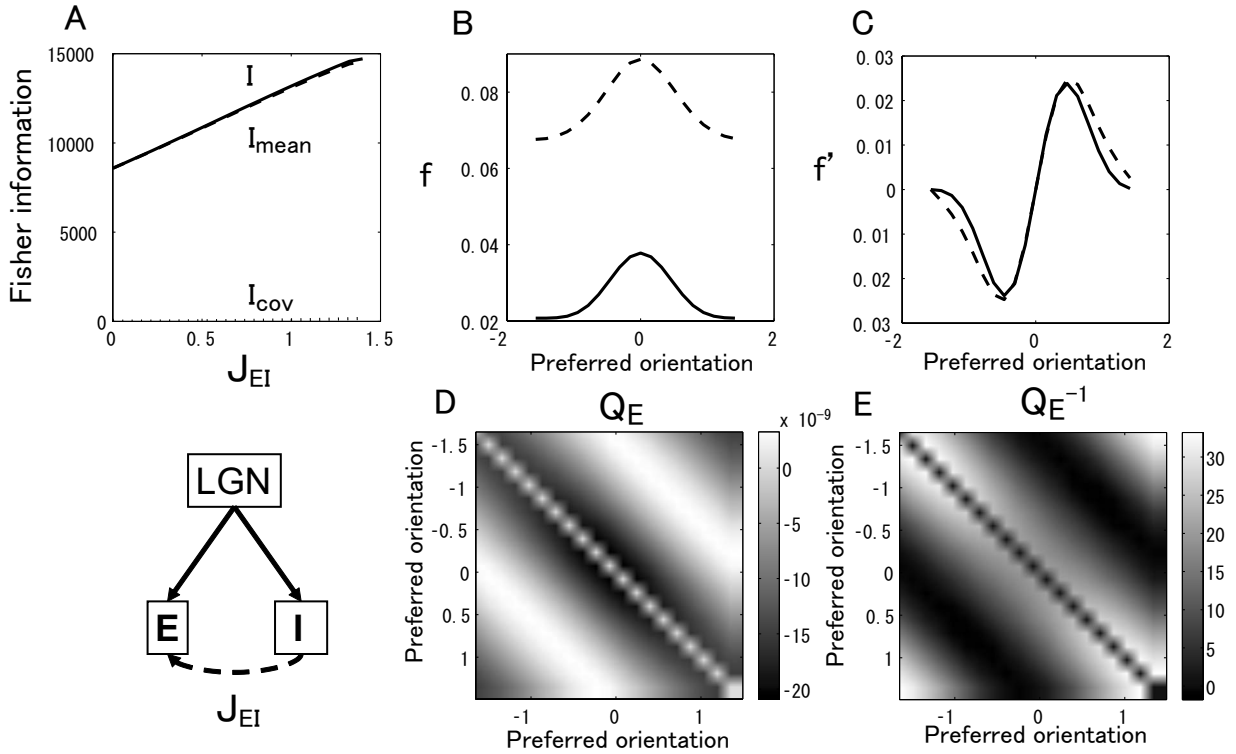

FIG. 6. (a) Effects of lateral inhibitions on Fisher information when the escape function is a threshold-linear function. J_{EE} is set to 0. Solid line: Fisher information I, dashed line: I_{mean}, dotted line: I_{cov}. [(b) and (c)] Mean firing rates, (a) $\mathbf{f}$, and derivatives of mean firing rates, (b) $\mathbf{f}'$, of V1 excitatory neurons. Solid lines plot $\mathbf{f}$ and $\mathbf{f}'$ when J_{EI}=1.4. Dashed lines plot $\mathbf{f}$ and $\mathbf{f}'$ when there is no lateral inhibition, i.e., J_{EI}=0. [(d) and (e)] Grayscale plots of covariance matrix, (d) $\mathbf{Q}_E$, and inverse of covariance matrix, (e) $\mathbf{Q}_E^{-1}$, of V1 excitatory neurons when J_{EI}=1.4. Diagonal elements were set to 0 to enable visualization. Note that scales of gray color maps are different in panels (d) and (e).

effects that correlations have on the Fisher information are stronger than the beneficial effects caused by the change in $\mathbf{f}'$. As a result, the recurrent excitations decrease the Fisher information.

Figure 3(a) shows the Fisher information when the strength of the lateral inhibitions, J_{EI}, varies. In contrast to sigmoid functions, lateral inhibitions increase the Fisher information. As we can see by comparing Figs. 6(b)–6(e) with Figs. 3(b)–3(e), the main effects of the change in $\mathbf{f}'$ and correlations on the Fisher information are the same. That is, correlations increase the Fisher information and the change in $\mathbf{f}'$ decreases the Fisher information. However, for the threshold-linear function, the beneficial effects of correlations on the Fisher information are stronger than the adverse effects caused by the change in $\mathbf{f}'$. As a total effect, the lateral inhibitions increase the Fisher information in this case.

Finally, we investigated how excitations and inhibitions in combination affect the accuracy of a population code. Figure 7(a) shows the Fisher information when the strengths of the recurrent excitations, J_{EE}, and lateral inhibitions, J_{EI}, vary. As in the sigmoid function case, the so-called marginal phase [12,19] was not included in the explored parameter regions shown in Fig. 7. From Fig. 7(a), we can see that the Fisher information increases as J_{EI} increases and the Fisher information decreases as J_{EE} increases. Figure 7(b) shows the width of the tuning curves of V1 excitatory neurons when J_{EE} and J_{EI} vary. Here, the tuning curves become sharper as J_{EI} increases and become broader as J_{EE} increases. As in the sigmoid function case, we can also find parameter regions where the Fisher information increases when sharpening occurs [region I in Fig. 7(c)]. In this region, inhibition is stronger than excitation (see discussion).

VII. DISCUSSION

We described a theoretical framework for investigating how lateral connections affect the accuracy of a population code. In our framework, the Fisher information can be analytically computed in a network of spike response models [8,14]. Some previous studies, in which the Fisher information was computed in realistic network models of spiking neurons, relied on numerical methods because of the difficulty of computing correlations, that take a substantial amount of time to calculate [5,6]. Our approach greatly reduced this time cost and enabled us to extensively investigate the various parameters of the network models.

With our framework, we investigated the effects of lateral connections on population coding in a network model of orientation selectivity in V1. The Fisher information depends on both the form of the tuning curves and correlation structures. Because lateral connections simultaneously change tuning curves and correlations, we need to take both effects on the Fisher information into consideration. We found that the effects conflict with each other in our neuron models. Whether or not lateral connections increase the Fisher infor-

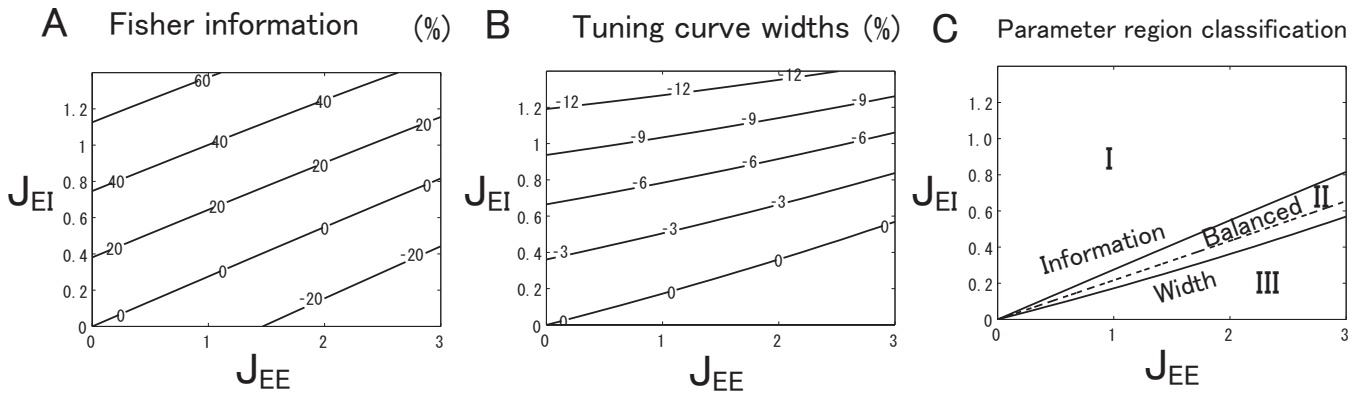

FIG. 7. Threshold-linear escape function case. (a) Contour plots of Fisher information when strengths of recurrent connections and lateral inhibitions, J_{EE} and J_{EI}, varied. Values on contour lines indicate percent increase or decrease in Fisher information compared with that obtained for network without lateral connections ($J_{EE}=J_{EI}=0$). (b) Contours plot of tuning curve widths when strengths of recurrent connections and lateral inhibitions, J_{EE} and J_{EI}, varied. Values on contour lines indicate percent increase or decrease in width compared with that obtained for network without lateral connections ($J_{EE}=J_{EI}=0$). Fitting of tuning curves with a Gaussian function, $f=f_0 \exp(\theta^2/\sigma^2)+C$, gave σ as width of tuning curves. (c) Classification of parameter regions based on Fisher information and tuning curve widths. Two solid lines are contour line of Fisher information (panel A) when there was no increase or decrease when strengths of recurrent connections and lateral inhibitions varied and of tuning curve widths (panel B) when there was no increase or decrease. In region I, Fisher information increases and tuning curves get sharper. In region II, Fisher information decreases and tuning curves get sharper. In region III, Fisher information decreases and tuning curves get broader. Dashed line indicates point at which peak firing rate of tuning curves does not change, i.e., point at which excitation and inhibition are balanced. Within parameter regions below dashed line, excitation is dominant. Within parameter regions above dashed line, inhibition is dominant.

mation strongly depends on the intrinsic properties of a model neuron, i.e., the escape function. In the present paper, we considered two simple but typical rate functions [8]. When the escape function is a sigmoid function, we found that the recurrent excitations increase the Fisher information and the lateral inhibitions decrease the Fisher information. When the escape function is a threshold-linear function, the opposite situation holds. That is, the recurrent excitations decrease the Fisher information and the lateral inhibitions increase the Fisher information. An important implication of this finding for real neurons is that the effects of recurrent excitation or inhibition strongly depend on the escape function, i.e., the neuronal input-output relationship [22–24]. To clarify how excitation and inhibition affect the accuracy of the population code in a real nervous system, we need to consider more realistic neuron models determined by physiological experiments. As it has been reported that the spike response model can capture the behavior of realistic neurons by fitting model parameters [8,11], the theoretical framework described in this paper provides a promising approach.

Some previous studies reported that sharpening tuning curves through Mexican-hat connectivities led to a severe loss of information [5,6]. They emphasized the adverse effects of correlation structures induced by Mexican-hat connectivities. However, by systematically changing the strengths of excitations and inhibitions, we found parameter regions where sharpening of tuning curves via Mexican-hat connectivities led to an increase in information. Our results revealed that even if correlation structures induced by Mexican-hat connectivities negatively affected the accuracy of population codes, the accuracy of a population code could be improved when the positive effects of the change in tuning curves overcame the negative effects. In the parameter regions where the accuracy of the population code was improved, excitation (or inhibition) was relatively stronger than inhibition (or excitation). Recent experimental and theoretical studies have shown that excitation and inhibition are nearly balanced in V1 [20,21]. In our model, the coding efficiency decreases as the strength of recurrent connectivities increases in the parameter regions where excitation and inhibition are balanced (Figs. 4 and 7). Further investigation is needed to elucidate the coding efficiency of V1 neurons in realistic parameter regions of recurrent connectivities. This is left for future work.

In this paper, we considered rate-based Fisher information under the assumption that the main information carriers in the brain are firing rates. However, there is a possibility that the precise spike timing as well as the spike count is used in the brain for decoding information on stimuli [25]. Comparing the rate-based Fisher information with the spike-based Fisher information [26], which is the amount of information when the individual spike timings of neurons are available, is an interesting issue that we intend to pursue.

ACKNOWLEDGMENTS

This work was partially supported by Grants-in-Aid for Scientific Research (Grants No. 18079003, No. 20240020, and No. 20650019) of the Ministry of Education, Culture, Sports, Science, and Technology of Japan (to M.O.). M.O. was supported by Grant-in-Aid for JSPS (Grant No. 08J08950).

APPENDIX A: CALCULATION OF CORRELATION FUNCTIONS

In this appendix, we describe the details of calculating correlation functions. First, we derive the time-delayed cross

correlations at equilibrium, $C_{ij}(\tau)$ [Eq. (20)]. By expanding $g(u_i)$ around the noise average of $\hat{u}_i$ [Eq. (8)], $C_{ij}(t,t+\tau) = \langle \delta S_i(t) g[u_j(t+\tau)] \rangle$ [Eq. (19)] can be written as

$$\langle \delta S_i(t) g[u_j(t+\tau)] \rangle = \langle g[\langle \hat{u}_j(t+\tau) \rangle + \eta_j(t'_j)] \delta S_i(t) \rangle + \sum_{\tau'=1}^{\infty} \sum_{k \neq j}^{N} J_{jk} \epsilon_{jk}(\tau') \langle g'[\langle \hat{u}_j(t+\tau) \rangle + \eta_j(t'_j)] \delta S_i(t) \delta S_k(t+\tau-\tau') \rangle, \quad \text{(A1)}$$

where $t'_j = t+\tau-t_j^{(f)}$, and we ignore terms of higher order than $1/N$. Taking the average for the refractory function $\eta_j(t'_j)$ and $S_i(t)$, the first term in Eq. (A1) can be computed as

$$\begin{aligned}
&\langle g[\langle \hat{u}_j(t+\tau) \rangle + \eta_j(t'_j)] \delta S_i(t) \rangle \\
&= \sum_{t'_j=1}^{\infty} \sum_{S_i(t)} P[t'_j, S_i(t)] g[\langle \hat{u}_j(t+\tau) \rangle + \eta_j(t'_j)] \delta S_i(t) \\
&= g[\langle \hat{u}_j(t+\tau) \rangle] \sum_{t'_j=\tau_{abs}+1}^{\infty} \sum_{S_i(t)} P[t'_j, S_i(t)] \delta S_i(t) \\
&= g[\langle \hat{u}_j(t+\tau) \rangle] \sum_{S_i(t)} \left\{ P[S_i(t)] - \sum_{t'_j=1}^{\tau_{abs}} P[t'_j, S_i(t)] \right\} \delta S_i(t) \\
&= -g[\langle \hat{u}_j(t+\tau) \rangle] \sum_{S_i(t)} \sum_{t'_j=1}^{\tau_{abs}} P[S_j(t+\tau-t'_j)=1, S_i(t)] \delta S_i(t) \\
&= -g[\langle \hat{u}_j(t+\tau) \rangle] \sum_{t'_j=1}^{\tau_{abs}} C_{ij}(t, t+\tau-t'_j), \quad \text{(A2)}
\end{aligned}$$

where $P(t'_j)$ is the probability that the last spike of neuron j occurred at $t+\tau-t'_j$, that is, $P(t'_j) = P[S_j(t+\tau-t'_j)=1, S_j(t+\tau-t'_j+1)=0, \ldots, S_j(t+\tau-1)=0]$. In the above calculation, we used the property of the absolute refractory period that when $t'_j \leq \tau_{abs}$, the joint probability $P[t'_j, S_i(t)]$ can be simply written as $P[S_j(t+\tau-t'_j)=1, S_i(t)]$.

Similarly, taking the average for $\eta_j(t'_j)$, $S_i(t)$, and $S_k(t+\tau-\tau')$, the second term in Eq. (A1) can be computed as

$$\begin{aligned}
&\langle g'[\langle \hat{u}_j(t+\tau) \rangle + \eta_j(t'_j)] \delta S_i(t) \delta S_k(t+\tau-\tau') \rangle \\
&= \sum_{t'_j=1}^{\infty} \sum_{S_i, S_k} P[t'_j, S_i(t), S_k(t+\tau-1)] g'[\langle \hat{u}_j(t+\tau) \rangle + \eta_j(t'_j)] \delta S_i(t) \delta S_k(t+\tau-\tau') \\
&= g'[\langle \hat{u}_j(t+\tau) \rangle] \sum_{S_i, S_k} \left\{ P[S_i(t), S_k(t+\tau-\tau')] - \sum_{t'_j=1}^{\tau_{abs}} P[t'_j, S_i(t), S_k(t+\tau-\tau')] \right\} \delta S_i(t) \delta S_k(t+\tau-\tau') \\
&= g'[\langle \hat{u}_j(t+\tau) \rangle] \left[C_{ik}(t, t+\tau-\tau') - C_{ik}(t, t+\tau - \tau') \sum_{t'_j=1}^{\tau_{sbs}} \langle S_j(t+\tau-t'_j) \rangle \right], \quad \text{(A3)}
\end{aligned}$$

where we assume that $i \neq k$ and ignore the three-point cross correlations, $\langle \delta S_i(t) \delta S_j(t+\tau-t'_j) \delta S_k(t+\tau-\tau') \rangle$, because these are order of $1/N^{3/2}$. When $i=k$, we replace the cross correlation, $C_{ik}(t, t+\tau-\tau')$, in Eq. (A3) with the autocorrelation, $A_i(t, t+\tau-\tau')$. Substituting Eqs. (A2) and (A3) into Eq. (A1), we obtain the dynamics of the time-delayed cross correlations,

$$\begin{aligned}
C_{ij}(t, t+\tau) = &- g[\langle \hat{u}_j(t+\tau) \rangle] \sum_{t'_j=1}^{\tau_{abs}} C_{ij}(t, t+\tau-t'_j) \\
&+ \left[1 - \sum_{t'_j=1}^{\tau_{abs}} \langle S_j(t+\tau-t'_j) \rangle \right] g'[\langle \hat{u}_j(t+\tau) \rangle] \sum_{\tau'}^{\infty} \left[\sum_{k \neq j,i} J_{jk} \epsilon_{jk}(\tau') C_{ik}(t, t+\tau-\tau') + J_{ji} A_i(t, t+\tau-\tau') \right]. \quad \text{(A4)}
\end{aligned}$$

Taking the limit $t \to \infty$ in Eq. (A4), we obtain the time-delayed cross correlations at equilibrium [Eq. (20)].

In the same way as we derive the time-delayed cross correlations, we can obtain the dynamics of the equal-time cross-correlation functions, $C_{ij}(t,t)$,

$$\begin{aligned}
C_{ij}(t,t) = &\, g[\langle \hat{u}_i(t) \rangle] g[\langle \hat{u}_j(t) \rangle] \sum_{t'_i=1}^{\tau_{abs}} \sum_{t'_j=1}^{\tau_{abs}} C_{ij}(t-t'_i, t-t'_j) \\
&+ g'[\langle \hat{u}_i(t) \rangle] g[\langle \hat{u}_j(t) \rangle] \left[-1 + \sum_{t'_i=1}^{\tau_{abs}} \langle S_i(t-t'_i) \rangle \right], \\
&\sum_{t'_j=1}^{\tau_{abs}} \sum_{\tau}^{\infty} \left[\sum_{k \neq i,j} J_{ik} \epsilon_{ik}(\tau) C_{kj}(t-\tau, t-t'_j) + J_{ij} \epsilon_{ij}(\tau) A_j(t-\tau, t-t'_j) \right] + g'[\langle \hat{u}_j(t) \rangle] g[\langle \hat{u}_i(t) \rangle] \\
&\times \left[-1 + \sum_{t'_j=1}^{\tau_{abs}} \langle S_j(t-t'_j) \rangle \right], \\
&\sum_{t'_i=1}^{\tau_{abs}} \sum_{\tau}^{\infty} \left[\sum_{k \neq i,j} J_{jk} \epsilon_{jk}(\tau) C_{ki}(t-\tau, t-t'_i) + J_{ji} \epsilon_{ji}(\tau) A_i(t-\tau, t-t'_i) \right] + g'[\langle \hat{u}_i(t) \rangle] g'[\langle \hat{u}_j(t) \rangle] \\
&\times \left[1 - \sum_{t'_i=1}^{\tau_{abs}} \langle S_i(t-t'_i) \rangle \right] \left[1 - \sum_{t'_j=1}^{\tau_{abs}} \langle S_j(t-t'_j) \rangle \right],
\end{aligned}$$

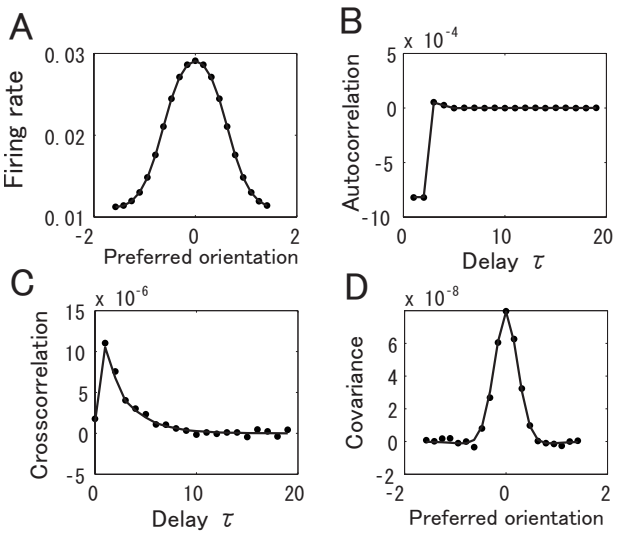

FIG. 8. Mean firing rates and correlation functions obtained from simulations (dots) compared with theory (solid line). The mean firing rates and correlation functions are estimated from the simulations over 10^8 time steps. Parameters of connections are J_{EE}=20.0, J_{EI}=5.0, J_{IE}=20.0, and J_{II}=5.0. (a) Mean firing rates of the V1 excitatory neurons. (b) Autocorrelation function $A_i(\tau)$ of the V1 excitatory neuron with preferred orientation 0 rad. (c) Cross-correlation function $C_{ij}(\tau)$ between a V1 excitatory neuron with preferred orientation $-\pi/20$ rad and a V1 excitatory neuron with preferred orientation 0 rad. (d) The mean firing rate correlations $Q_{E,ij}$ between a V1 excitatory neuron with preferred orientation 0 rad and V1 excitatory neurons with preferred orientations from $-\pi/2$ to $9\pi/20$.

$$\left(\sum_{\tau,\tau'}^{\infty} \sum_{k\neq i} \sum_{l\neq j,k} J_{ik}\epsilon_{ik}(\tau)J_{jl}\epsilon_{jl}(\tau')C_{kl}(t-\tau,t-\tau') + \sum_{\tau,\tau'}^{\infty} \sum_{k\neq i} J_{ik}\epsilon_{ik}(\tau)J_{jk}\epsilon_{jk}(\tau')A_k(t-\tau,t-\tau') \right), \quad \text{(A5)}$$

where we ignore terms of higher order than $1/N$. By taking the limit $t\to\infty$ in Eq. (A5), we obtain the equal-time cross correlations at equilibrium [Eq. (17)].

APPENDIX B: EMPIRICAL ESTIMATES OF FISHER INFORMATION

We checked whether the analytically computed Fisher information was consistent with empirical estimates of Fisher information from data sampled from the network model, as was done in previous studies [6,27]. To estimate the Fisher information, we train a linear decoder

$$\hat{\phi} = \mathbf{w}\mathbf{r} + b, \quad \text{(B1)}$$

where $\mathbf{w}$ is a weight vector, b is a scalar, and $\mathbf{r}$ is the firing rate of the V1 excitatory neurons. $\mathbf{w}$ and b are optimized for two values of orientation ϕ_1 and ϕ_2 which differ by a small angle $\delta\theta$. Training is done by using the conjugate gradient method [27]. Once training is completed, an estimate of Fisher information can be computed by the following equation:

$$I_{\mathrm{LOLE}} = \frac{[(\langle\hat{\phi}_2\rangle - \langle\hat{\phi}_1\rangle)/\delta\phi]^2}{(\sigma^2_{\hat{\phi}_2} + \sigma^2_{\hat{\phi}_1})/2}, \quad \text{(B2)}$$

where $\delta\phi=\phi_2-\phi_1$, $\langle\phi_i\rangle$ is the mean, and $\sigma_{\phi_i}(i=1,2)$ is the variance of the estimates on test data (see [6] for details). I_{LOLE} provides an estimate of the fist term of the Fisher information in Eq. (27), I_{mean}, because I_{mean} gives an upper bound on the decoding error of the optimal linear estimator of the stimulus θ [28,29]. I_{mean} is called linear Fisher information.

Before we applied the above method of estimating the Fisher information to data sampled from our network model,

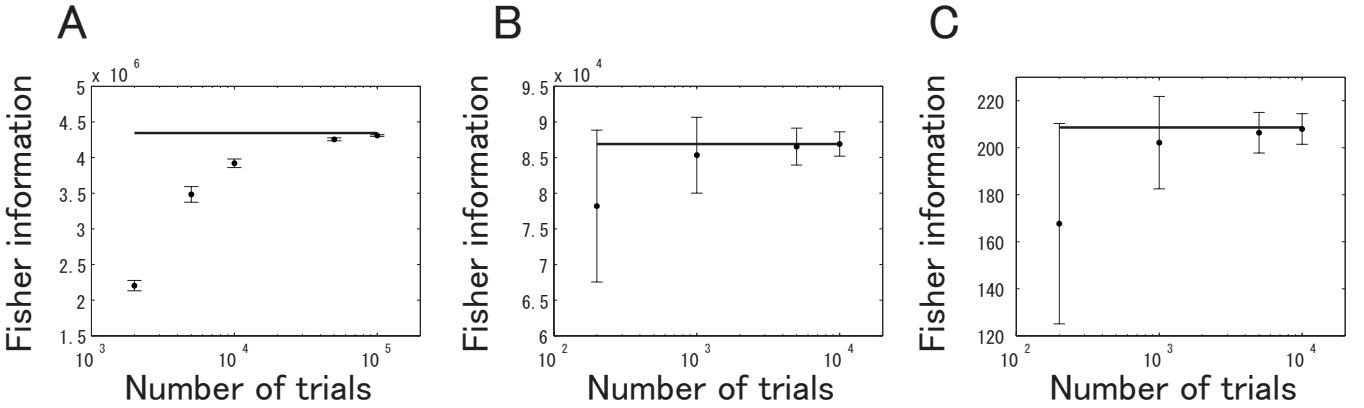

FIG. 9. Empirical estimates of Fisher information by using I_{LOLE} when the number of trials used for the estimation varies. The number of neurons is 1000 in panel (a), 20 in panel (b), and 20 in panel (c). In panels (a) and (b), data sampled from the Gaussian distribution [Eq. (B3)] are used. In panel (c), data obtained by simulating our network model are used. Dots represent the mean of I_{LOLE} and the error bars represent the standard deviation of I_{LOLE}. The horizontal solid line shows the actual value of the Fisher information.

we examined how much data are needed to accurately estimate the Fisher information in simple toy examples. We considered N neurons whose firing rates obey Gaussian statistics. The firing rates of the neurons responding to stimulus ϕ are

$$r_i = f_0 \exp(a\{\cos[2(\theta_i - \phi)]\}) + \eta_i, \tag{B3}$$

where $\theta_i = -\pi/2 + i\pi/N$ and η_i are independent Gaussian random variables with zero mean and variance σ^2. We generated M trials for both orientations $\phi_1 = 0$ and $\phi_2 = 0.01$. Half of those trials were used for training and the other half of trials were used for evaluating the mean and the variance of the estimates of the orientations. The parameter values are $f_0 = 20$, $a = 0.23$, and $\sigma = 0.1$. The number of neurons was $N = 1000$. We computed I_{LOLE} ten times and evaluated the mean and the standard deviation of I_{LOLE}. Figure 9(a) shows the mean and the standard deviation of I_{LOLE} when the number of trials M varies. From Fig. 9(a), we can see that the Fisher information would be largely underestimated if the number of trials was not much larger than the number of neurons N. When we used 2000 trials, the Fisher information was underestimated by about 50%. We needed more than 10 000 trials to obtain 90% of the actual Fisher information. Noting the amount of data needed for the accurate estimation shown in Fig. 9(a), we can say that a relatively small number of trials were used to estimate the Fisher information in some of the previous studies [6,27]. In our network model, we have 2000 V1 excitatory neurons. Thus, it is hard to accurately estimate the Fisher information contained in all V1 excitatory neurons with I_{LOLE}. Instead of computing the Fisher information from all V1 excitatory neurons, we considered computing it from 20 selected ones. We chose one neuron from each subpopulation and gathered $K_E = 20$ of them, where K_E is number of subpopulations (see Sec. V for details of the network architecture).

We considered a case in which a sigmoid function is used for the escape function $g(u)$. The model parameters are shown in Fig. 8. Note that we did not change the total number of neurons in the network model; we only changed the number of neurons from which we computed the Fisher information. In this case, the analytically computed linear Fisher information in 20 selected excitatory neurons is $I_{\mathrm{mean}} = 209$. We generated 10 000 trials for two orientations $\phi_1 = 0$ and $\phi_2 = 0.01$ by simulating our network model. 10 000 trials gave us a good estimate of the Fisher information when the number of neuron was 20, judging from the same test in the simple toy example described above [Fig. 9(b)]. We randomly chose one neuron from each subpopulation consisting of $G_E = 100$ neurons with the same orientation preference and computed I_{LOLE} from the data of the 20 excitatory neurons. We randomly chose 20 neurons 1000 times and computed I_{LOLE} in those 1000 different populations of neurons. Figure 9(c) plots the mean and standard deviation of I_{LOLE} when the number of trials varies. When the number of trials is 10 000, the mean of I_{LOLE} was $\langle I_{\mathrm{LOLE}} \rangle = 208$ and the standard deviation was $\sigma_{I_{\mathrm{LOLE}}} = 6.51$. We thus could say that the empirical estimate of Fisher information was consistent with the analytically computed Fisher information.

APPENDIX C

Table of parameters (Tables I–III).

TABLE I. Neuron parameters.

u	Membrane potential
u_r	Resting potential
τ_s	Time constant of postsynaptic potential
τ_{abs}	Absolute refractory period

TABLE II. Tuning curve parameters.

h_0	Input potential of LGN neurons
ϕ	Orientation of stimulus
a	Width of tuning curves in LGN neurons

TABLE III. Network parameters.

σ_E	Range of excitation in V1
σ_I	Range of inhibition in V1
J_{EL}	Strength of synaptic connections from LGN neurons to V1 excitatory neurons
J_{IL}	Strength of synaptic connections from LGN neurons to V1 inhibitory neurons
J_{EE}	Strength of synaptic connections from V1 excitatory neurons to V1 excitatory neurons
J_{EI}	Strength of synaptic connections from V1 inhibitory neurons to V1 excitatory neurons
J_{IE}	Strength of synaptic connections from V1 excitatory neurons to V1 inhibitory neurons
J_{II}	Strength of synaptic connections from V1 inhibitory neurons to V1 inhibitory neurons

[1] L. F. Abbott and P. Dayan, Neural Comput. **11**, 91 (1999).
[2] H. S. Seung and H. Sompolinsky, Proc. Natl. Acad. Sci. U.S.A. **90**, 10749 (1993).
[3] H. Sompolinsky, H. Yoon, K. Kang, and M. Shamir, Phys. Rev. E **64**, 051904 (2001).
[4] K. Zhang and T. J. Sejnowski, Neural Comput. **11**, 75 (1999).
[5] M. Spiridon and W. Gerstner, Network **12**, 409 (2001).
[6] P. Series, P. E. Latham, and A. Pouget, Nat. Neurosci. **7**, 1129 (2004).
[7] M. A. Paradiso, Biol. Cybern. **58**, 35 (1988).
[8] W. Gerstner and W. Kistler, *Spiking Neuron Models* (Cambridge University Press, Cambridge, England, 2002).
[9] I. Ginzburg and H. Sompolinsky, Phys. Rev. E **50**, 3171 (1994).
[10] C. Meyer and C. van Vreeswijk, Neural Comput. **14**, 369 (2002).
[11] W. Kistler, W. Gerstner, and J. L. van Hemmen, Neural Comput. **9**, 1015 (1997).
[12] R. Ben-Yishai, R. L. Bar-Or, and H. Sompolinsky, Proc. Natl. Acad. Sci. U.S.A. **92**, 3844 (1995).
[13] D. C. Somers, S. B. Nelson, and M. Sur, J. Neurosci. **15**, 5448 (1995).
[14] W. Gerstner and J. L. van Hemmen, Network **3**, 139 (1992).
[15] J. Macke, P. Berens, A. S. Ecker, A. S. Tolias, and M. Bethge, Neural Comput. **21**, 397 (2009).
[16] S. M. Kay, *Fundamentals of Statistical Signal Processing: Estimation Theory* (Cambridge University Press; Prentice-Hall, Englewood Cliffs, NJ, 1993).
[17] D. H. Hubel and T. N. Wiesel, J. Physiol. **160**, 106 (1962).
[18] T. Cover and J. Thomas, *Elements of Information Theory* (Wiley, New York, 1991).
[19] *Methods in Neuronal Modeling*, edited by C. Koch and I. S. Segev, 2nd ed. (The MIT Press, Cambridge, MA, 1998).
[20] J. Mariño, J. Schummers, D. C. Lyon, L. Schwabe, O. Beck, P. Wiesing, K. Obermayer, and M. Sur, Nat. Neurosci. **8**, 194 (2005).
[21] M. Stimberg, K. Wimmer, R. Martin, L. Schwabe, J. Mariño, J. Schummers, D. C. Lyon, M. Sur, and K. Obermayer, Cereb. Cortex **19**, 2166 (2009).
[22] R. Azouz, C. M. Gray, L. G. Nowak, and D. A. McCormick, Cereb. Cortex **7**, 534 (1997).
[23] B. Ahmed, J. C. Anderson, R. J. Douglas, K. A. Martin, and D. Whitteridge, Cereb. Cortex **8**, 462 (1998).
[24] C. E. Stafstrom, P. C. Schwindt, and W. E. Crill, J. Neurophysiol. **52**, 264 (1984).
[25] S. Panzeri, R. S. Peterson, S. R. Schultz, M. Lebedev, and M. E. Diamond, Neuron **29**, 769 (2001).
[26] T. Toyoizumi, K. Aihara, and S. Amari, Phys. Rev. Lett. **97**, 098102 (2006).
[27] M. I. Chelaru and V. Dragoi, Proc. Natl. Acad. Sci. U.S.A. **105**, 16344 (2008).
[28] M. Shamir and H. Sompolinsky, Neural Comput. **16**, 1105 (2004).
[29] P. E. Latham, S. Deneve, and A. Pouget, J. Physiol. Paris **97**, 683 (2003).